

Ab initio downfolding study of the iron-based ladder superconductor BaFe₂S₃

Ryotaro Arita,^{1,2} Hiroaki Ikeda,³ Shiro Sakai,¹ and Michi-To Suzuki¹

¹RIKEN Center for Emergent Matter Science, 2-1 Hirosawa, Wako, Saitama 351-0198, Japan

²ERATO Isobe Degenerate π -Integration Project, Tohoku University, Aoba-ku, Sendai 980-8578, Japan

³Department of Physics, Ritsumeikan University, 1-1-1 Noji-higashi, Kusatsu, Shiga 525-8577, Japan

(Received 10 June 2015; published 26 August 2015)

Motivated by the recent discovery of superconductivity in the iron-based ladder compound BaFe₂S₃ under high pressure, we derive low-energy effective Hamiltonians from first principles. We show that the complex band structure around the Fermi level is represented only by the Fe 3d_{xz} (mixed with 3d_{xy}) and 3d_{x²-y²} orbitals. The characteristic band degeneracy allows us to construct a four-band model with the band unfolding approach. We also estimate the interaction parameters and show that the system is more correlated than the 1111 family of iron-based superconductors. Provided the superconductivity is mediated by spin fluctuations, the 3d_{xz}-like band plays an essential role, and the gap function changes its sign between the Fermi surface around the Γ point and that around the Brillouin-zone boundary.

DOI: 10.1103/PhysRevB.92.054515

PACS number(s): 74.20.Mn, 74.25.Jb, 74.62.Fj, 74.70.-b

I. INTRODUCTION

Since the discovery of superconductivity in fluorine-doped LaFeAsO [1], a variety of iron pnictides and chalcogenides have been found to exhibit superconductivity with high transition temperatures (T_c). In these compounds, Fe ions commonly form a two-dimensional (2D) network. This fact raises an intriguing and fundamental question whether the square network is essential for the high T_c superconductivity and what happens in different geometries. In the case of the cuprates, it was discovered that the ladder compound (Sr,Ca)₁₄Cu₂₄O₄₁ becomes a superconductor under pressure ~ 3 GPa [2]. This experimental observation has stimulated various theoretical studies on superconductivity in quasi-1D systems. Interestingly, it has been recently found that a ladder compound BaFe₂S₃ becomes a superconductor under high pressure ~ 10 GPa [3]. In the phase diagram, the superconducting phase resides next to a magnetic insulating phase, in which the spin correlation is antiferromagnetic along the ladder and ferromagnetic along the rung. The maximum T_c is as high as 14 K. The superconducting transition in BaFe₂S₃ is of great interest, since we may have a chance to pin down the origin/mechanism of the high T_c superconductivity in iron-based superconductors (FeSC) by investigating the commonalities and differences between the 2D and quasi-1D systems.

Recently, motivated by the experimental works on superconductivity in the single-layer potassium-doped iron selenide (110) film (which can be viewed as a weakly coupled ladder system) [4] or ladder compounds such as BaFe₂Se₃ [5–10] and CsFe₂Se₃ [11] (which do not exhibit superconductivity), a variety of theoretical studies have been reported [12–18]. However, studies for BaFe₂S₃ based on *ab initio* calculation are yet to be performed. In this study, we derive low-energy effective Hamiltonians for BaFe₂S₃ from first principles, focusing on the Fe 3d bands around the Fermi level (E_F). We find that a d_{xz}-like orbital, a linear combination of d_{xz} and d_{xy}, forms two Fermi (electron) pockets around $k_z = 0$ and a d_{x²-y²}-like orbital forms a Fermi (hole) pocket around $k_z = \pi$. The effective energy bands obtained with the two orbital models are further depicted in the unfolded Brillouin zone

(BZ), in which one of the electron pockets is placed around the BZ boundary of $k'_z = \pi$. Since the magnetic instability is strong at $q'_z \sim \pi$ in the extended BZ, the d_{xz}-like orbital should be active for spin-fluctuation-mediated superconductivity. We also estimate the values of interaction parameters in the effective Hamiltonian, such as the Hubbard U and Hund's coupling J . We show that BaFe₂S₃ is more strongly correlated than the 1111 compounds.

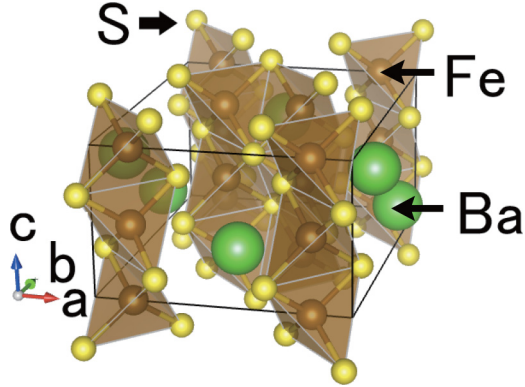
II. CRYSTAL STRUCTURE

In Fig. 1, we show the crystal structure of BaFe₂S₃. We see that Fe atoms form two-leg ladders running along the c axis. In the following calculation for ambient pressure, we used the lattice constants a, b, c and the atomic positions of Ba, Fe, and S reported in Ref. [19]. Namely, the lattice constants a, b , and c are 8.78, 11.23, and 5.29 Å, respectively. The space group is *Cmcm*, and the atomic positions of Ba(4c), Fe(8e), S(4c), and S(8g) are (0.0, 0.686, 0.25), (0.154, 0.0, 0.0), (0.0, 0.116, 0.25), and (0.208, 0.378, 0.25), respectively. In the phase diagram of temperature (T) and pressure (P), the superconducting phase has a domelike shape and T_c is highest around $P = 12.4$ GPa. For $P = 12.4$ GPa, a, b , and c shrink to 96.0%, 92.0%, and 96.6% of those at ambient pressure, respectively [19,20]. Since the atomic configuration under pressure is yet to be reported, in the present calculation, we just change the lattice constants.

III. BAND STRUCTURE, FERMI SURFACE AND PROJECTED DENSITY OF STATES

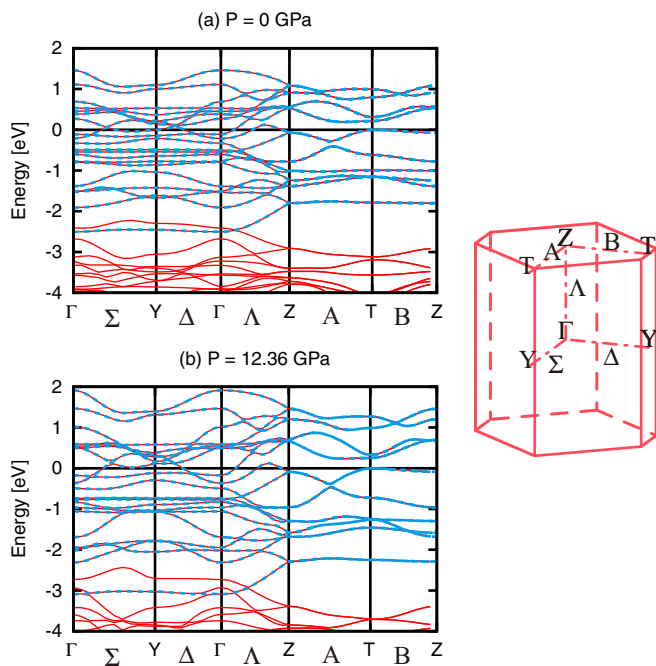
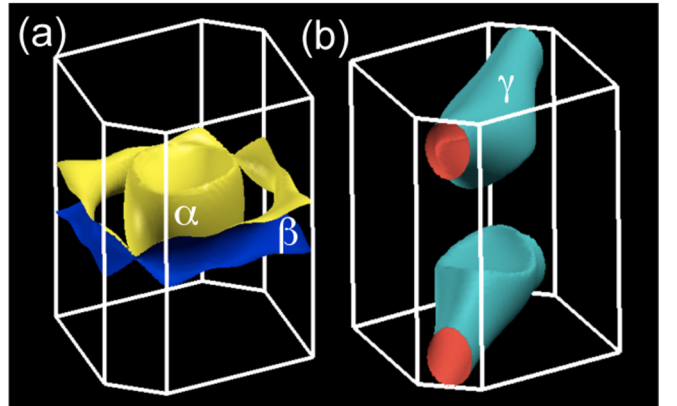
We performed density functional calculation for the experimental crystal structure [21] with the QUANTUM ESPRESSO package [22]. Here we employ the exchange correlation functional by Perdew *et al.* [23]. The wave functions are expanded by plane waves up to a cutoff energy of 40 Ry, and an $8 \times 8 \times 8$ k mesh in the first Brillouin zone is used.

Based on the band calculation, we further constructed Wannier functions for these bands using the WANNIER90

FIG. 1. (Color online) Crystal structure of BaFe_2S_3 .

package [24]. The resulting spreads of the $d_{3z^2-r^2}$, d_{xz} , d_{yz} , $d_{x^2-y^2}$, and d_{xy} orbitals are 2.35, 3.51, 3.13, 2.40, and 3.14 \AA^2 for ambient pressure, and 2.91, 4.01, 3.35, 2.73, and 3.43 \AA^2 for $P = 12.4 \text{ GPa}$. If we compare the Wannier spreads of the 2D FeSC (Table III in Ref. [25]), we see that at $P = 0$ the Wannier functions are as localized as those of LiFeAs, but at $P = 12.4 \text{ GPa}$ they are more delocalized than those of BaFe_2As_2 .

In Fig. 2, we show the band dispersion obtained by the Wannier interpolation (blue dashed curves) with that from the density functional calculation (red solid curves). Since the unit cell contains four Fe atoms, there are 20 Fe 3d bands around the Fermi level. We see that the bandwidth of the Fe 3d states for $P = 12.4 \text{ GPa}$ is larger than that for $P = 0$ by $\sim 25\%$. We list the resulting hopping integrals in the Supplemental

FIG. 2. (Color online) Band structure for ambient pressure (a) and $P = 12.4 \text{ GPa}$ (b). The original (Wannier interpolated) band dispersion is shown by red solid (blue dashed) curves. In the inset, we show the Brillouin zone.FIG. 3. (Color online) Fermi pockets α and β (a) and γ (b) of BaFe_2S_3 for $P = 0$.

Material [26]. As is expected from the crystal structure shown in Fig. 1, the band structure is dispersive along the k_z axis (from the Γ to Z point). The transfer integral is largest between the nearest-neighbor $d_{3z^2-r^2}$ orbitals along the ladder (the c axis), and its amplitude is $\sim 0.56 \text{ eV}$. For $P = 12.4 \text{ GPa}$, it becomes 0.64 eV . These values are larger than the nearest-neighbor transfer integrals for the 2D FeSC (see Tables IV–VII in Ref. [25]). On the other hand, the interladder transfer integrals are small, so that the band structure of BaFe_2S_3 is quasi-one-dimensional along the k_z axis. Nevertheless, since the dominant transfer integrals along the c axis are large, the bandwidth of BaFe_2S_3 turns out to be a similar value to that of 2D FeSC (see Fig. 4 in Ref. [25]). As for the on-site energies of $d_{3z^2-r^2}$, d_{xz} , d_{yz} , $d_{x^2-y^2}$, and d_{xy} , they are 7.44, 8.00, 8.03, 7.69, and 7.95 eV (where $E_F = 8.19 \text{ eV}$) for $P = 0$, and 9.37, 10.02, 9.98, 9.62, and 9.89 eV (where $E_F = 10.22 \text{ eV}$) for $P = 12.4 \text{ GPa}$. The size of the crystal field splitting is similar to that of the 2D FeSC.

In Fig. 3, we show the Fermi surface for $P = 0$. There are two electron pockets around $k_z = 0$, hereafter called α and β , and one hole pocket around $k_z = \pi$, called γ . For $P = 12.4 \text{ GPa}$, the β pocket significantly shrinks, while the α pocket is quite robust against the external pressure. The energy band lying just below $E_F (= 0 \text{ eV}$ hereafter) around the T points at $P = 0$ crosses the Fermi level under pressure, resulting in another tiny pocket for $P = 12.4 \text{ GPa}$.

We plot the projected density of states for the 3d orbitals in Fig. 4. We see that $d_{3z^2-r^2}$ does not contribute to the low-energy states. On the other hand, the Fermi pockets α , β , and γ are mainly composed of d_{xy} , d_{xz} , and $d_{x^2-y^2}$, respectively. The contribution of d_{yz} to these pockets is subdominant. As for the electron filling n of $d_{3z^2-r^2}$, d_{xz} , d_{yz} , $d_{x^2-y^2}$, and d_{xy} , they are 0.61, 0.54, 0.56, 0.76, and 0.50 for $P = 0$, and 0.60, 0.51, 0.62, 0.76, and 0.53 for $P = 12.4 \text{ GPa}$. Since n of the $d_{x^2-y^2}$ orbital is quite high, $d_{x^2-y^2}$ should be inactive magnetically. It is interesting to note that n of $d_{3z^2-r^2}$ in the 2D FeSC is ~ 0.75 (see Table II in Ref. [25]), and the orbital extends in the direction perpendicular to the Fe plane as $d_{x^2-y^2}$ in BaFe_2S_3 does. So far, several studies have pointed out that $d_{3z^2-r^2}$ in the 2D FeSC does not play a crucial role in the magnetism and superconductivity [27–30].

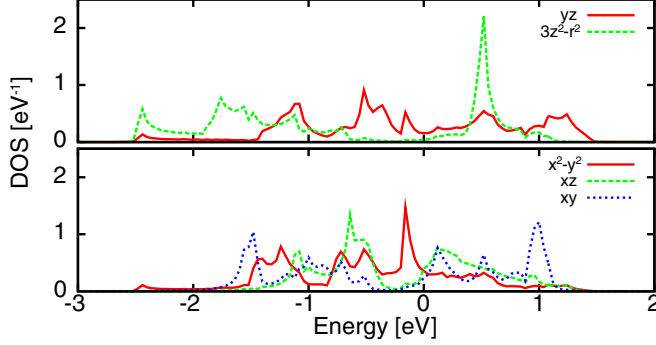


FIG. 4. (Color online) Projected density of states for $P = 0$. While the amplitude of d_{yz} and $d_{3z^2-r^2}$ around E_F is not large, the contributions from $d_{x^2-y^2}$, d_{xz} , and d_{xy} are significant.

IV. TWO-ORBITAL MODEL AND BZ UNFOLDING

We now further try to simplify the five-orbital (20-band) model. We have found that the energy dispersion around E_F can be represented by a two-orbital (eight-band) model in which the Wannier functions are mainly composed of two orbitals, i.e., $d_{x^2-y^2}$ and d_{xz} hybridized with d_{xy} . We hereafter call the Wannier functions $w_{x^2-y^2}$ and w_{xz} . To construct the Wannier functions, the inner (outer) window is set to be $(-0.3 \text{ eV}, 0.2 \text{ eV})$ [$(-1.2 \text{ eV}, 1.5 \text{ eV})$] with respect to E_F [31]. In Fig. 5(a), we compare the original *ab initio* bands and the Wannier interpolated bands for ambient pressure. We obtained a similar result for $P = 12.4 \text{ GPa}$ (not shown). We list the resulting hopping integrals for the two-orbital model in the Supplemental Material [26].

Interestingly, we can further simplify the current model by unfolding the BZ, as was done for the 1111 compound [32]. Indeed, if we introduce a local gauge transformation for one of the two orbitals to change its sign, we can expand the band dispersion from Γ to Z [see Fig. 5(b)] [33]. Then the model is simplified to a four-band model.

In the 2D FeSC, both the hole and electron pockets consist of more than two orbitals. Here let us look at the orbital character of the Fermi surface of BaFe_2S_3 . In Fig. 6, we plot the band dispersion of the four-band model.

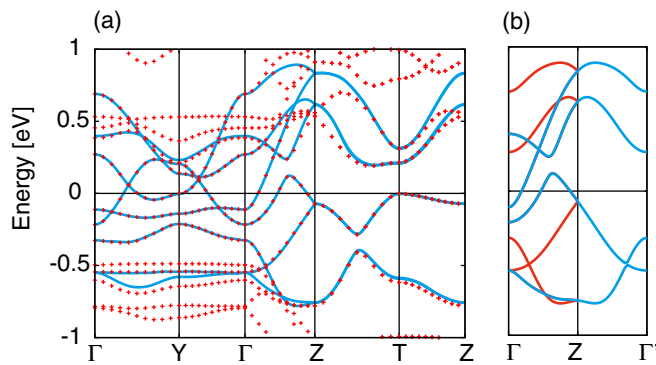


FIG. 5. (Color online) (a) Band dispersion of the effective two-orbital (eight-band) model for $P = 0$ (blue solid curves). The original *ab initio* band structure is shown by dotted curves. (b) Band dispersion in the extended (unfolded) BZ.

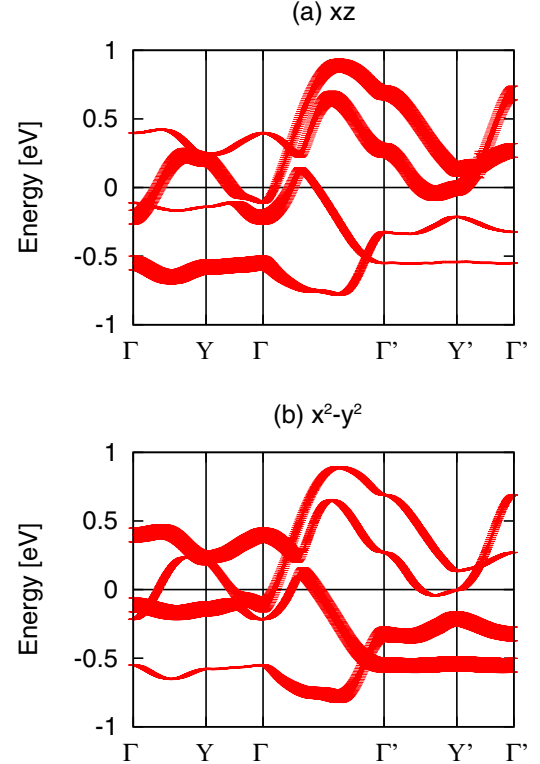


FIG. 6. (Color online) Band dispersion of the four-band model for $P = 0$. The weight of each orbital is represented by the width of the curve.

of the each orbital is represented by the width of the curves. We can see that w_{xz} forms electron pockets around Γ and Y' (the Fermi pockets α and β in the original BZ). On the other hand, the hole pocket sitting between Γ and Γ' (the γ pocket in the original BZ) consists of w_{xz} and $w_{x^2-y^2}$. The far (near) side of the pocket from Γ has a dominant $w_{x^2-y^2}$ (w_{xz}) character.

V. LINDHARD FUNCTION

In the 2D FeSC, the Lindhard function $\chi^0(\mathbf{q})$ has a peak around $(\pi, 0, 0)$ and $(0, \pi, 0)$ in the extended BZ [34], which is compatible with the stripe-type antiferromagnetic order. This fact has caused hot debates on which of either the localized spin picture or the itinerant picture is more appropriate for describing the magnetic properties of 2D FeSC [35–41]. Thus it is interesting to see whether the peak position of $\chi^0(\mathbf{q})$ for BaFe_2S_3 agrees with the Bragg peak observed in the experiment.

In Fig. 7, we plot $\chi_{ij}^0(\mathbf{q})$ for the five-orbital model in the extended Brillouin zone. Here i and j ($=1, 2$) specify the Fe atom in the unit cell. We see that the correlation along the ladder ($i = j$) is stronger than that along the rung $i \neq j$, and $\chi^0(\mathbf{q})$ does not depend on q_x and q_y significantly. As for the q_z' dependence, $\chi^0(\mathbf{q})$ has larger values in the plane of $q_z' = \pi$ than $q_z' = 0$, due to the nesting between the α and β pockets in Fig. 3. Note that the β pocket moves to the plane of $q_z' = \pi$ in the extended Brillouin zone. For $P = 12.4 \text{ GPa}$, although the β pocket shrinks, we confirmed that the contribution from the particle-hole scattering between α and β is still dominant. This q_z' dependence of $\chi^0(\mathbf{q})$ is consistent with

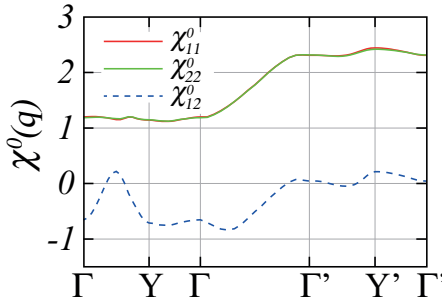


FIG. 7. (Color online) Wave number dependence of the Lindhard function for the five-orbital model at $P = 0$.

the experiment in that the intraorbital spin correlation is antiferromagnetic along the ladder. As for the correlation along the rung, it is ferromagnetic, since ferromagnetically coupled spin configuration $S_1 + S_2$ (where S_i is the spin at the i th Fe atom in the unit cell) has stronger correlation than $S_1 - S_2$ (note that $\chi_{12}^0 > 0$ at $\mathbf{q} = Y'$). This is also consistent with the experiment.

On the other hand, for the interladder correlation, $\chi^0(\mathbf{q})$ is peaked at Y' , while the Bragg peak in experiment is observed to be located at $0.5\mathbf{b}_1 + 0.5\mathbf{b}_2$ (\mathbf{b}_1 and \mathbf{b}_2 are the reciprocal primitive vectors) [3]. This result suggests that the interladder correlation cannot be explained simply in terms of Fermi surface nesting.

VI. SUPERCONDUCTIVITY

Since the superconducting phase resides next to the anti-ferromagnetic phase, let us here assume that the superconductivity is mediated by spin fluctuations. Then the pairing interaction is strong at $q_z' = \pi$, and favors a pairing gap function having different signs between the Fermi pockets α and β . The active band for superconductivity is w_{xz} in this scenario, because both α and β are made from w_{xz} . On the other hand, $w_{x^2-y^2}$ makes a pocket around $q_z' = \pm\pi/2$, but should be passive for the superconductivity. In the 2D FeSC, it has been proposed that d_{xy} is important to understand the material dependence of the superconducting transition temperature [42–47]. It is interesting to note that both w_{xz} in BaFe₂S₃ and d_{xy} in the 2D FeSC extend in the direction of pnictogen/chalcogen sites, and are almost half-filled in the five-orbital model.

For 2D FeSC, the orbital fluctuation mechanism has been extensively studied [48–50]. While it is an interesting future problem to study whether orbital fluctuations mediate superconductivity in BaFe₂S₃, there is a notable difference between the quasi-1D and 2D systems. In the case of the 2D FeSC, d_{yz} and d_{xz} are essential for the orbital-fluctuation mechanism. While these orbitals correspond to d_{xy} and d_{yz} in BaFe₂S₃, these are irrelevant in the two-orbital model.

VII. ELECTRON CORRELATIONS

Let us move on to the electron correlations in BaFe₂S₃. By means of the constrained random phase approximation [51], we estimate the values of the Hubbard U and the Hund's coupling J in the five-orbital model. We used the density

TABLE I. Hubbard U and Hund's J in the five-orbital model for $P = 0$ GPa.

U (eV)	xy	yz	$3z^2 - r^2$	xz	$x^2 - y^2$
xy	3.35	2.42	2.34	2.33	3.16
yz	2.42	3.26	2.89	2.30	2.54
$3z^2 - r^2$	2.34	2.89	3.79	2.77	2.44
xz	2.33	2.30	2.77	2.99	2.43
$x^2 - y^2$	3.16	2.54	2.44	2.43	3.86
J (eV)	xy	yz	$3z^2 - r^2$	xz	$x^2 - y^2$
xy	—	0.50	0.67	0.48	0.22
yz	0.50	—	0.32	0.46	0.55
$3z^2 - r^2$	0.67	0.32	—	0.30	0.71
xz	0.48	0.46	0.30	—	0.51
$x^2 - y^2$	0.22	0.55	0.71	0.51	—

response code of Elk [52,53]. In the calculation of the charge susceptibility, we took 100 unoccupied bands and $4 \times 4 \times 4\mathbf{k}$ and \mathbf{q} meshes. The double Fourier transform of the charge susceptibility was done with the cutoff of $|\mathbf{G} + \mathbf{q}| = 2, 3, 4, 5$, and 6 (1/a.u.) with \mathbf{G} being the reciprocal vector, from which we estimated the values extrapolated to the limit of $|\mathbf{G} + \mathbf{q}| \rightarrow \infty$. In Table I, we list the resulting values of U and J for $P = 0$. If we compare these values (and the ratio J/U , which is important to measure the electron correlations in 2D FeSC [54]) with those of the 2D FeSC [25,55], we see that they are as strong as those of LiFeAs. The pressure dependence of U and J is not so strong and they become smaller only by ~6–7% under the pressures up to $P = 12.4$ Pa. These results suggest that BaFe₂S₃ is more strongly correlated than the 1111 compounds [25,56]. This observation is consistent with the fact that the ordered moment of BaFe₂S₃ is about $1.3\mu_B$, which is larger than that of LaFeAsO [56,57].

VIII. CONCLUSION

We have studied the electronic structure of BaFe₂S₃ from first principles. Detailed analysis of the full Fe orbital model revealed that the Fermi surfaces are represented only by the two Fe orbitals, i.e., w_{xz} and $w_{x^2-y^2}$. Provided that the superconductivity is mediated by spin fluctuations, w_{xz} , which corresponds to d_{xy} in the 2D FeSC, is essential for superconductivity. In fact, they have the following common features: (i) they extend in the direction of pnictogen/chalcogen sites, (ii) they are nearly half-filled, and (iii) they form disconnected Fermi pockets around Γ and near the boundary of the BZ, between which pairing interaction mediated by stripe-type antiferromagnetic spin fluctuation works effectively [58]. Concerning the electron correlations, it is stronger than those of LaFeAsO or LaFePO.

ACKNOWLEDGMENTS

We thank K. Ohgushi, H. Takahashi, J. Yamaura, and Y. Nambu for providing us their result [3,19] prior to its publication and Y. Nomura for useful discussions. This work is financially supported by JSPS [Grants No. 15H03696 (R.A.), No. 26800179 (S.S.), and No. 15K17713 (M.S.)].

- [1] Y. Kamihara, T. Watanabe, M. Hirano, and H. Hosono, *J. Am. Chem. Soc.* **130**, 3296 (2008).
- [2] M. Uehara, T. Nagata, J. Akimitsu, H. Takahashi, N. Môri, and K. Kinoshita, *J. Phys. Soc. Jpn.* **65**, 2764 (1996).
- [3] H. Takahashi, A. Sugimoto, Y. Nambu, T. Yamauchi, Y. Hirata, T. Kawakami, M. Avdeev, K. Matsabayashi, F. Du, C. Kawashima *et al.*, *Nat. Mater.* (2015), doi:10.1038/nmat4351.
- [4] W. Li, H. Ding, P. Zhang, P. Deng, K. Chang, K. He, S. Ji, L. Wang, X. Ma, J. Wu *et al.*, *Phys. Rev. B* **88**, 140506 (2013).
- [5] J. M. Caron, J. R. Neilson, D. C. Miller, A. Llobet, and T. M. McQueen, *Phys. Rev. B* **84**, 180409 (2011).
- [6] A. Krzton-Maziopa, E. Pomjakushina, V. Pomjakushin, D. Sheptyakov, D. Chernyshov, V. Svitlyk, and K. Conder, *J. Phys.: Condens. Matter* **23**, 402201 (2011).
- [7] H. Lei, H. Ryu, A. I. Frenkel, and C. Petrovic, *Phys. Rev. B* **84**, 214511 (2011).
- [8] B. Saparov, S. Calder, B. Sipos, H. Cao, S. Chi, D. J. Singh, A. D. Christianson, M. D. Lumsden, and A. S. Sefat, *Phys. Rev. B* **84**, 245132 (2011).
- [9] J. M. Caron, J. R. Neilson, D. C. Miller, K. Arpino, A. Llobet, and T. M. McQueen, *Phys. Rev. B* **85**, 180405 (2012).
- [10] Y. Nambu, K. Ohgushi, S. Suzuki, F. Du, M. Avdeev, Y. Uwatoko, K. Munakata, H. Fukazawa, S. Chi, Y. Ueda *et al.*, *Phys. Rev. B* **85**, 064413 (2012).
- [11] F. Du, K. Ohgushi, Y. Nambu, T. Kawakami, M. Avdeev, Y. Hirata, Y. Watanabe, T. J. Sato, and Y. Ueda, *Phys. Rev. B* **85**, 214436 (2012).
- [12] W. Li, C. Setty, X. Chen, and J. Hu, *Front. Phys.* **9**, 465 (2014).
- [13] M. V. Medvedev, I. A. Nekrasov, and M. V. Sadovskii, *JETP Lett.* **95**, 33 (2012).
- [14] Q. Luo and E. Dagotto, *Phys. Rev. B* **89**, 045115 (2014).
- [15] Q. Luo, K. Foyevtsova, G. D. Samolyuk, F. Reboredo, and E. Dagotto, *Phys. Rev. B* **90**, 035128 (2014).
- [16] W. Lv, A. Moreo, and E. Dagotto, *Phys. Rev. B* **88**, 094508 (2013).
- [17] Q. Luo, A. Nicholson, J. Rincón, S. Liang, J. Riera, G. Alvarez, L. Wang, W. Ku, G. D. Samolyuk, A. Moreo *et al.*, *Phys. Rev. B* **87**, 024404 (2013).
- [18] E. Dagotto, *Rev. Mod. Phys.* **85**, 849 (2013).
- [19] Y. Hirata, S. Maki, J.-i. Yamaura, T. Yamauchi, and K. Ohgushi, *arXiv:1507.06047*.
- [20] M.-T. Suzuki, R. Arita, and H. Ikeda, *Phys. Rev. B* **92**, 085116 (2015).
- [21] For the sensitivity of the electronic structure of 2D iron-based superconductors to the crystal structure (see, e.g., Refs. [42,59–61]).
- [22] P. Giannozzi, S. Baroni, N. Bonini, M. Calandra, R. Car, C. Cavazzoni, D. Ceresoli, G. L. Chiarotti, M. Cococcioni, I. Dabo *et al.*, *J. Phys.: Condens. Matter* **21**, 395502 (2009).
- [23] J. P. Perdew, K. Burke, and M. Ernzerhof, *Phys. Rev. Lett.* **77**, 3865 (1996).
- [24] A. A. Mostofi, J. R. Yates, Y.-S. Lee, I. Souza, D. Vanderbilt, and N. Marzari, *Comput. Phys. Commun.* **178**, 685 (2008).
- [25] T. Miyake, K. Nakamura, R. Arita, and M. Imada, *J. Phys. Soc. Jpn.* **79**, 044705 (2010).
- [26] See Supplemental Material at <http://link.aps.org/supplemental/10.1103/PhysRevB.92.054515> for tight-binding parameters in the effective Hamiltonian.
- [27] L. de' Medici, G. Giovannetti, and M. Capone, *Phys. Rev. Lett.* **112**, 177001 (2014).
- [28] N. Lanatà, H. U. R. Strand, G. Giovannetti, B. Hellsing, L. de' Medici, and M. Capone, *Phys. Rev. B* **87**, 045122 (2013).
- [29] T. Misawa, K. Nakamura, and M. Imada, *J. Phys. Soc. Jpn.* **80**, 023704 (2011).
- [30] T. Misawa, K. Nakamura, and M. Imada, *Phys. Rev. Lett.* **108**, 177007 (2012).
- [31] I. Souza, N. Marzari, and D. Vanderbilt, *Phys. Rev. B* **65**, 035109 (2001).
- [32] K. Kuroki, S. Onari, R. Arita, H. Usui, Y. Tanaka, H. Kontani, and H. Aoki, *Phys. Rev. Lett.* **101**, 087004 (2008).
- [33] The unfolded band is not exactly the same as the original band for general k points. For another way to unfold the Brillouin zone, see e.g., Refs. [62–66].
- [34] I. I. Mazin, D. J. Singh, M. D. Johannes, and M. H. Du, *Phys. Rev. Lett.* **101**, 057003 (2008).
- [35] P. Dai, J. Hu, and E. Dagotto, *Nat. Phys.* **8**, 709 (2012).
- [36] J. Paglione and R. L. Greene, *Nat. Phys.* **6**, 645 (2010).
- [37] R. Arita and H. Ikeda, *J. Phys. Soc. Jpn.* **78**, 113707 (2009).
- [38] P. Hansmann, R. Arita, A. Toschi, S. Sakai, G. Sangiovanni, and K. Held, *Phys. Rev. Lett.* **104**, 197002 (2010).
- [39] A. Toschi, R. Arita, P. Hansmann, G. Sangiovanni, and K. Held, *Phys. Rev. B* **86**, 064411 (2012).
- [40] M. Liu, L. W. Harriger, H. Luo, M. Wang, R. A. Ewings, T. Guidi, H. Park, K. Haule, G. Kotliar, S. M. Hayden *et al.*, *Nat. Phys.* **8**, 376 (2012).
- [41] H. Park, K. Haule, and G. Kotliar, *Phys. Rev. Lett.* **107**, 137007 (2011).
- [42] K. Kuroki, H. Usui, S. Onari, R. Arita, and H. Aoki, *Phys. Rev. B* **79**, 224511 (2009).
- [43] D. J. Scalapino, *Rev. Mod. Phys.* **84**, 1383 (2012).
- [44] P. J. Hirschfeld, M. M. Korshunov, and I. Mazin, *Rep. Prog. Phys.* **74**, 124508 (2011).
- [45] C. Platt, W. Hanke, and R. Thomale, *Adv. Phys.* **62**, 453 (2013).
- [46] A. Chubukov, *Annu. Rev. Condens. Matter Phys.* **3**, 57 (2012).
- [47] F. Wang and D.-H. Lee, *Science* **332**, 200 (2011).
- [48] H. Kontani and S. Onari, *Phys. Rev. Lett.* **104**, 157001 (2010).
- [49] S. Onari and H. Kontani, *Phys. Rev. Lett.* **109**, 137001 (2012).
- [50] Y. Nomura, K. Nakamura, and R. Arita, *Phys. Rev. Lett.* **112**, 027002 (2014).
- [51] F. Aryasetiawan, M. Imada, A. Georges, G. Kotliar, S. Biermann, and A. I. Lichtenstein, *Phys. Rev. B* **70**, 195104 (2004).
- [52] See <http://elk.sourceforge.net/>.
- [53] A. Kozhevnikov, A. Eguiluz, and T. Schulthess, in SC'10 Proceedings of the 2010 ACM/IEEE International Conference for High Performance Computing, Networking, Storage, and Analysis (unpublished), p. 1.
- [54] K. Haule and G. Kotliar, *New J. Phys.* **11**, 025021 (2009).
- [55] K. Nakamura, R. Arita, and M. Imada, *J. Phys. Soc. Jpn.* **77** (2008).
- [56] Z. Yin, K. Haule, and G. Kotliar, *Nat. Mater.* **10**, 932 (2011).
- [57] N. Qureshi, Y. Drees, J. Werner, S. Wurmehl, C. Hess, R. Klingeler, B. Büchner, M. T. Fernández-Díaz, and M. Braden, *Phys. Rev. B* **82**, 184521 (2010).

- [58] K. Kuroki and R. Arita, *Phys. Rev. B* **64**, 024501 (2001).
- [59] V. Vildosola, L. Pourovskii, R. Arita, S. Biermann, and A. Georges, *Phys. Rev. B* **78**, 064518 (2008).
- [60] I. I. Mazin, M. D. Johannes, L. Boeri, K. Koepernik, and D. J. Singh, *Phys. Rev. B* **78**, 085104 (2008).
- [61] O. Andersen and L. Boeri, *Ann. Phys. (N.Y.)* **523**, 8 (2011).
- [62] T. Berlijn, P. J. Hirschfeld, and W. Ku, *Phys. Rev. Lett.* **109**, 147003 (2012).
- [63] T. Berlijn, H.-P. Cheng, P. J. Hirschfeld, and W. Ku, *Phys. Rev. B* **89**, 020501 (2014).
- [64] W. Ku, T. Berlijn, and C.-C. Lee, *Phys. Rev. Lett.* **104**, 216401 (2010).
- [65] T. Berlijn, C.-H. Lin, W. Garber, and W. Ku, *Phys. Rev. Lett.* **108**, 207003 (2012).
- [66] S. Konbu, K. Nakamura, H. Ikeda, and R. Arita, *J. Phys. Soc. Jpn.* **80**, 123701 (2011).